THE DISTRIBUTION OF SHALE IN SANDSTONES AND ITS EFFECT UPON POROSITY

By

E. C. Thomas
Shell Oil Company
New Orleans, Louisiana

S. J. Stieber
Butler, Miller & Lents
Houston, Texas

ABSTRACT

A shale volume parameter derived from the response of the gamma ray log in shaly sands is often used to correct the responses of other logs for the effects of the shale. The correlation of a gamma ray parameter to shale volume is usually presented as one direct relationship. However, because the shale can be distributed through the sand in different ways, such as laminated, dispersed, structural, or any combination of these, one may expect varying gamma ray responses dependent upon geometry. We show that each of these configurations can involve a different response from the gamma ray and this variable response can be used to determine the shale configuration. A gamma ray parameter vs. porosity crossplot can then be used to determine shale configuration, sand fraction and sand porosity; the derived equations can be used for implicit solution when processing digital log data. These configurational data can be combined with electric log parameters to determine the oil saturation of the net sand. These log derived parameters are herein verified by direct comparison to rubber sleeve core data.

The sparcity of porosity logs in many of the older South Louisiana fields often necessitates that other available log data be correlated to porosity. One log which is generally available is the gamma ray collar log which is used to perforate the well. Thus, empirical gamma ray response - Density log porosity correlations in a particular reservoir are developed using recent penetrations, and this correlation is applied to the older gamma ray logs to determine a reservoir-wide porosity distribution. This simple approach is fruitful for reservoirs which are found in Tertiary sand-shale sequences and usually will not apply to more complicated mineralogies involving carbonates. An example of this type of correlation is shown in Figure 1.

T

It is assumed from the above that shale is the main destroyer of sand porosity and it is therefore reasonable to expect the gamma ray to correlate to porosity. However, if sorting or mineralization are the dominant factors in sand porosity variation, then no simple gamma ray response correlation to porosity should be found because the gamma ray responds to the presence or absence of radioactive minerals. We must learn how the shale is distributed in the sand, for this distribution governs the productivity.

There are three broad categories which describe how shale can be distributed in a sand:

1. Laminated - layers of shale within the sand.

2. Dispersed - shale on the sand grains, or pore filling.

3. Structural - sand sized shale particles in load-bearing positions within the rock.

Of course there can be any combinations of these categories. Thus, to quantitatively determine shale content and distribution we have developed a simple mathematical model which relates gamma ray response to shale distribution and concentration. The five main assumptions in the model are the following:

1. There are only two rock types, a high porosity "clean" sand and a low porosity "pure" shale. The observed in situ porosities are generated by mixing the two.

2. Within the interval investigated, there is no change in shale type and the shale mixed in the sand is mineralogically the same as the "pure" shale sections above and below the sand.

3. The gamma ray responds to the number of radioactive events in a material and thus its mass. The shale fractions we wish to determine are a function of volume. We assume for the Tertiary basins that both sands and shales have comparable grain densities, thus, the radioactivity will be proportional to volume.

4. Constant background radiation will be assumed to be present in all measurements.

5. Counting yields will not change as rock types are intermixed.

The components of the system are sand and shale, thus, we have chosen to use shale rather than clay minerals, even though it is the clay

which contains the bulk of the radioactive material. We believe shaly sands and shales are mineralogically similar because both facies are derived from the same source material, carried by the same river and emptied into the same basin. The differentiation between sands and shales begins as the particles settle at differing rates according to their size and transport energy and not mineral type. (This is not rigorously true but, except for heavy minerals, very vesicular minerals, or colloids the differences in density are not dominant.) Thus, we feel the porosity destroying material introduced into a sand stratum will be of the same composition as the shales above and below the sand stratum. Of course, this will not be true for the diagenetic alteration of feldspars into clay within the sand stratum.

We define the subscripts a = sand and b = shale. Take a solid block of sand material and place it near an instrument capable of measuring the gamma rays emitted, we observe a counting rate, R_a, expressed as

$$R_a^* = Y_a A_a \qquad (1)$$

where Y is the counting yield, A is the activity and the asterisk indicates that $\phi_a = 0$.

Now if we crush the solid and build a porous rock with the pieces, we introduce a void space, V_a. Express V_a in terms of the fraction of the total volume of rock, V_t, then $V_a/V_t = \phi_a$, the pure sand rock porosity. The grain volume fraction, grainosity, is then χ_a, and $\chi_a = (1-\phi_a)$. If we now repeat the gamma ray detection experiment using this new porous rock, the counting rate observed is

$$R_a = (1-\phi_a)\ Y_a'\ A_a \qquad (2)$$

where the prime was added to denote a change in counting yield because of a geometry change in the material counted.

If we repeat the same crushing and construction experiment using the shale material, we observe

$$R_b = (1-\phi_b)\ Y_b'\ A_b\ . \qquad (3)$$

Let's now mix together quantities of the porous sand and shale, and assume the counting yield will not be significantly altered (Assumption No. 5). We will elaborate on the error caused by this assumption in Appendix 1. There are three independent ways to place the shale in the sand block and these are treated separately.

1. Dispersed shale (pore filling)

   Place some shale in the sand's pore space. We define the fraction of the total volume occupied by this shale as X_b.

T

Now if we count the gamma rays, we observe

$$R = (1-\phi_a)\ Y_a'\ A_a + X_b\ (1-\phi_b)\ Y_b'\ A_b. \tag{4}$$

If we substitute (2) and (3) into (4) we get

$$R = R_a + X_b\ R_b \tag{5}$$

or simply the observed count rate increases proportional to the amount of shale added to the pore systems.

If we are to apply this concept to borehole gamma ray measurements we must relate a defined parameter, γ, which correlates to porosity, in terms of X_b, the bulk volume fraction occupied by shale.

The value of γ in a sand stratum is defined in terms of the above parameters as

$$\gamma = \frac{R_b - R}{R_b - R_a} \tag{6}$$

where R_b is observed in the "purest" nearby shale, and R_a observed in the nearest "clean" sand.

Substituting (5) into (6), then

$$\gamma = \frac{R_b - (R_a + X_b\ R_b)}{R_b - R_a} \qquad = 1 - \frac{X_b\ R_b}{R_b - R_a} \tag{7}$$

For simplicity lets define

$$\zeta = \frac{R_b}{R_b - R_a} \tag{8}$$

which is a measure of how radioactive the sands are. The relation between γ and X_b then becomes

$$X_b = \frac{1 - \gamma}{\zeta} \tag{9}$$

when X_b is pore filling.

One point to note is that the minimum porosity available to the dispersed model is when shale completely fills all the original pore volume of the sand or when

$$X_b = \phi_a,$$

$$\phi \text{ min, dispersed} = \phi_a \times \phi_b. \tag{10}$$

When $X_b > \phi_a$, then equation (4) for the counting rate is not valid because we must remove sand grains to add shale. We derive this equation by starting with pure shale ($X_b = 1$) and work back to $X_b = \phi_a$. Thus, $R = (1-\phi_b)\ Y_b'A_b - X_a\ (1-\phi_b)\ Y_b'A_b + X_a\ (1-\phi_a)\ Y_a'A_a$. (11)

Substituting (2) and (3) into (11) we get

$$R = R_b - X_aR_b + X_aR_a. \tag{12}$$

Using $X_a = 1-X_b$, (12) rearranges to $R = R_b - (1-X_b)(R_b-R_a)$. (13)

Substituting (13) into (6), $\gamma = 1-X_b = X_a$. (14)

2. Laminated model

Now when we add shale to the sand stratum we must replace sand and its associated porosity, ϕ_a, with shale to keep a constant total volume of material. The amount of sand removed and shale added is X_b, the sand fraction. Thus

$$R = (1-\phi_a)\ Y_a'A_a - (1-\phi_a)\ Y_a'A_aX_b + (1-\phi_b)\ Y_bA_bX_b. \tag{15}$$

Substituting (2) and (3) into (15) yields

$$R = R_a + X_b\ (R_b-R_a). \tag{16}$$

If we substitute (16) into (6) then

$$\gamma = \frac{R_b - R_a - X_b\ (R_b-R_a)}{R_b - R_a} = 1-X_b = X_a\ . \tag{17}$$

Thus for the laminated model γ is the sand fraction.

3. Structural

When we add shale in structural positions we remove sand grains only. Thus the porosity increases with the amount of shale porosity that we add in place of the solid sand grain. Or

$$R = (1-\phi_a)\ Y_a'A_a - X_b\ (1-\phi_a)\ Y_a'A_a + X_b\ (1-\phi_b)\ Y_b'A_b \tag{18}$$

which is the same as (15). Thus, the γ to X_b relationship for structural shale is identical to that for the laminated model.

T

Now that we know the relation between γ and shale fraction, we can construct a theoretical γ-porosity relationship based on these three models.

1. Dispersed (pore filling) - we start with the total porosity of a or ϕ_a. We then add shale in the pore space, thus decreasing the porosity by the amount of grainosity of the shale.

$$\phi_{dis} = \phi_a - X_b\,(1-\phi_b) \text{ for } X_b < \phi_a, \text{ the available space} \qquad (19)$$

for shale.

The end points of this equation are easily fixed and are independent of any proposed relation between X_b and γ. When $X_b = 0$, $\phi_{dis_{max}} = \phi_a$ and when $X_b = \phi_a$, $\phi_{dis_{min}} = \phi_a\phi_b$.

Substituting (9) into (19)

$$\phi_{dis} = \phi_a - \frac{(1-\gamma)}{\zeta}\,(1-\phi_b). \qquad (20)$$

A reasonable number for ζ in South Louisiana sands is 1.25.* Thus the relation between these end points is linear with γ. The actual value of γ at $\phi_{dis_{min}}$ is difficult to define absolutely because of Assumption No. 5. The error caused by this assumption is discussed in Appendix 1. The porosity relation for the region when $X_b > \phi_a$ is derived just as is the radiation relationship by starting with pure shale and adding sand grains which have no porosity, thus reducing the total porosity by the value of sand added.

$$\phi_{dis} = \phi_b - X_a\phi_b = \phi_b - (1-X_b)\,\phi_b, \qquad (21)$$

when $X_b > \phi_a$.

Substituting (14) into (21) yields

$$\phi_{dis} = \phi_b - \gamma\phi_b. \text{ The relation is linear with } \gamma. \qquad (22)$$

When $\gamma = 0$, $\phi_{dis} = \phi_b$ and this is a fixed end point. γ_{max} in eq. (22) is limited as γ_{min} in eq. (20). However this number is difficult to fix as stated before. See Appendix 1.

2. Laminated - in this case we remove both the porosity and grainosity of the sand and replace it by the shale porosity and grainosity.

*This value is derived from eq. (8) using R_b = 100 API units and R_a = 20 API units.

$$\phi_{lam} = \phi_a - X_b\ (\phi_a) + X_b\ (\phi_b). \tag{23}$$

Substitute (17) into (23)

$$\phi_{lam} = \gamma\phi_a + (1-\gamma)\ \phi_b. \tag{24}$$

The end points are easily fixed when $\gamma = 1$, $\phi_{lam} = \phi_a$ and when $\gamma = 0$, $\phi_{lam} = \phi_b$. These end points are independent of γ-X_b relation and are firm. Also equation (24) demonstrates a linear relation between the two end points.

3. Structural - in this case we remove no sand porosity, only sand grainosity, and replace it with an equivalent bulk volume fraction of shale porosity,

$$\phi_{str} = \phi_a + X_b\ \phi_b. \tag{25}$$

Substitute (18) or (17) into (25)

$$\phi_{str} = \phi_a + (1-\gamma)\ \phi_b. \tag{26}$$

The maximum amount of structural shale which can be added equals the grainosity of the sand or $X_{max} = 1-\gamma_{min} = 1-\phi_a$. (27)

Notice that ϕ increases linearly with decreasing γ. This startling result is obvious upon inspection of the model and is the consequence of replacing the solid quartz grain with a corresponding volume of porous shale. The radiation at the maximum is a simple relation because no sand grains remain. However, the counting yield will be different than for pure shale. But if we use Assumption No. 5, then

$$R = \chi_a\ (1-\phi_b)\ Y_b'A_b = (1-\phi_a)\ R_b. \tag{28}$$

Then substituting (28) into (6)

$$\gamma = \frac{R_b - (1-\phi_a)R_b}{R_b-R_a} = \frac{R_b\ (\phi_a)}{R_b - R_a}. \tag{29}$$

Substituting (8) into (29)

$$\gamma = \zeta\ \ (\phi_a). \tag{30}$$

Thus (27) and (30) are not equal, again the consequences of Assumption No. 5. See Appendix 1.

T

In reality we do not have any of these pure models but rather we have a combination of the three. One simplification is to assume the amount of structural shale is too small to be significant and remove this possibility from the model. This simplification permits the response of a gamma ray-density log to be solved (graphically or algebraically) for sand fraction, sand porosity and shale distribution.

As an example we choose a Miocene reservoir in South Louisiana, where clean sand porosity is 33% and pure shale porosity is 15%. This is the same reservoir shown in Figure 1. We can then construct a γ-density porosity crossplot triangle limited by these data, using eq. (20), (22), and (24), shown in Figure 2. Eq. (26) is also presented.

This is done by fixing the $\gamma = 1$ point at $\phi = 33\%$, $\gamma = 0$ at 15%. A line drawn between these points is the laminated model limit expressed by eq. 24. The minimum ϕ for the dispersed is given by eq. 10 as $\phi_a \times \phi_b$ or 0.0495. Solution of eq. 20 for γ, using $\zeta = 1.25$, yields $\gamma = 0.588$. A line connecting this point to the $\gamma = 1$ point is the graphical approximation of eq. 22.

Isolaminous lines are added to Figure 2 by constructing lines parallel to the dispersed shale model line. The percent laminations is then read from the laminated model line as the percentage of the laminated model line substended by the isolaminous line measured from the $\gamma = 1.0$ apex. Isoporous lines are added to Figure 2 by constructing lines which connect the $\gamma = 0$ apex to the dispersed shale model line. The porosity of the sand laminae anywhere along a given line is read at its intercept on the dispersed shale model line. For a specific example, a FDC log in a thick sand reads $\phi = 28\%$ and $\gamma = 0.85$. Using Figure 2, we start at the $\phi = 28$, $\gamma = .85$ point, which is on an isolam corresponding to 10% shale laminations, then proceed up an isopor to the intercept on the dispersed shale model line of $\phi = 29.4$. Thus, for this example the bed is composed of 10% shale laminations and the porosity of the interbedded sand is 29.4%. We have illustrated this solution graphically, but of course it can be done algebraically.

We recently had the opportunity to test this hypothesis when we cored a well in South Louisiana which penetrated this same reservoir. Figure 3 shows the petrophysical log section across the reservoir. Figure 4 shows the oil saturation and porosity calculated for the entire interval. Figure 5 shows some of the core photographs, demonstrating the laminated nature of the sand. Note the good sand at the top and the extremely laminated material at the bottom. Figure 6 shows the corresponding FDC ϕ plotted versus stressed core porosity. The FDC ϕ is calculated using measured grain densities and fluid densities from the core adjusted to reservoir temperature and pressure. The good agreement in the clean sand is apparent, while a corresponding disparity appears in the lower laminated section. This is an artifact of biased sampling. Only the sand between the laminations was plugged for core analysis, thus giving misleading results.

Using the core photographs, the amount of sand and shale can be counted precisely and when a clean sand porosity of 31% (the average Ø from stressed core analysis) and pure shale porosity of 15% are assigned to the laminations, the average porosity as seen by the density log is reproduced. Conversely, from the gamma ray-density log porosity crossplot, the sand fraction and sand porosity matches that counted from the photographs and measurements in the lab.

Thus, if one knows he is in a laminated environment he can apply the laminated resistivity model;

$$\frac{1}{R_a} = \frac{f_{sd}}{R_{sd}} \times \frac{f_{sh}}{R_{sh}}$$

The value of R_a is read from the induction log, f_{sd} and f_{sh} are obtained from the crossplot, and R_{sh} takes from the induction log in a nearby shale zone. Then the actual value percent of R_{sd} and R_t of the sand can be calculated. The effect of using the true sand Ø and R_t to calculate S_o is shown in Figure 7. This is a repeat of Figure 4, with an overlay showing the change in calculated S_o in the heavily laminated zones. In most cases, the oil saturation increases. The effect shown here increases as the percent laminations increase to the point where the shale resistivity dominates the apparent resistivity, thereby condemning a zone which could produce hydrocarbons.

ACKNOWLEDGMENT

The authors wish to thank Shell Oil Company for granting permission to publish this work. We also thank B. E. Ausburn of Shell Oil Company who allowed us to use Figure 4 which he had prepared earlier. We appreciate the many discussions with our collegues who helped solidify many of the concepts presented.

SYMBOLS

A - activity, number of radioactive events

R - counting rate observed at a detector or the Resistivity.

V - void space

X - volume fraction of material

Y - counting yield, an experimental constant which relates the true activity to the number of events counted by the detector

a - subscript for clean sand

T

b - subscript for pure shale

f - fraction of bulk volume, used in Resistivity models

γ - defined by eq. 6 using counting rates in pure shales and clean sands. It is often the sand fraction.

ζ - defined by eq. 8 and is a measure of sand radioactivity.

ϕ - porosity, the void space of a rock expressed as a volume fraction of the total bulk volume.

χ - grainosity, the solid part of a rock expressed as a volume fraction of the total bulk volume.

APPENDIX 1

We realize that errors have been introduced to the model by many of our assumptions. However, these assumptions are necessary to arrive at the simple equations presented in the text. We feel justified in using assumption (5) because we are also assuming no fluid radioactivity and constant background in spite of unknown changes in borehole size and rugosity, cement type and placement, and detector type and size.

By assigning a few numbers to the equations we can explore the potential errors caused by assumption (5) and demonstrate the small error introduced by its acceptance.

Let's refer to Figure 2. The $\gamma = 1$ point is fixed by the uncertainty in determining ϕ_a from field measurements. But for the theoretical model we can set this number exactly, thus the $\gamma = 1$, $\phi = \phi_a$ apex is firm. Similarly for the $\gamma = 0$, $\phi = \phi_b$ apex. Equation (24) demonstrated that the equation which connects these two apexes is linear, thus the position of this line is firm within the confines of the other assumptions. The minimum ϕ available is fixed at $\phi_a\phi_b$. However, the value of γ at this point is less well known. Eq. (20) predicts $\gamma = .59$ while Eq. (22) predicts $\gamma = .67$. The actual value is probably between the two, thus the max error for ϕ_{dis} in the working area of the triangle (ϕ apparent $> \phi_b$) is ± 1.5 and the mean error about $\pm .5$. We feel this is acceptable for any practical application. For the structural shale model we have similar uncertainties in γ at the ϕ_{max} point. The value of ϕ_{max} is fixed at $\phi_a + \chi_a\phi_b$ or $\phi_a + (1-\phi_a)\,\phi_b = .43$. We can calculate $\gamma = .33$ from eq. (27) and $\gamma = .41$ from eq. (30). The ϕ error introduced by uncertainty in γ is less than $\pm .5$.

Thus, we feel the small uncertainties introduced by assuming no change in counting yield or background as we build our model are within the uncertainties in typical field applications and are therefore justified to simplify the treatment of the data.

BIOGRAPHICAL SKETCHES

E. C. THOMAS is a Senior Petrophysical Engineer and Section Leader for Shell's Coastal Division Petrophysical Engineering Section. He earned a B.S. in Chemistry from Louisiana State University in 1963 and a Ph.D. in Physical Chemistry from Stanford University in 1966. E.C. joined Shell in 1967 at the Exploration & Production Research Center in Houston after being on the faculty at Princeton University. At the Bellaire Research Center he was project leader for the formation evaluation group in the Petrophysical Engineering Section. In 1972 he was transferred to the Coastal Division in New Orleans and assumed his present position July 1974.

S. J. STIEBER is a Petroleum Engineer with Butler, Miller, and Lents in Houston. He earned a B.S. in Petroleum Engineering from the University of Southwestern Louisiana in 1963 and a M.S. in Petroleum Engineering from the University of Oklahoma in 1974. John has been employed by Amerada Petroleum Corporation in Lafayette and Oklahoma City and by Shell Oil Company in New Orleans. He served as Petrophysical Engineering Section Leader until June 1974 when he assumed his present position.

E.C.Thomas

S.J.Stieber

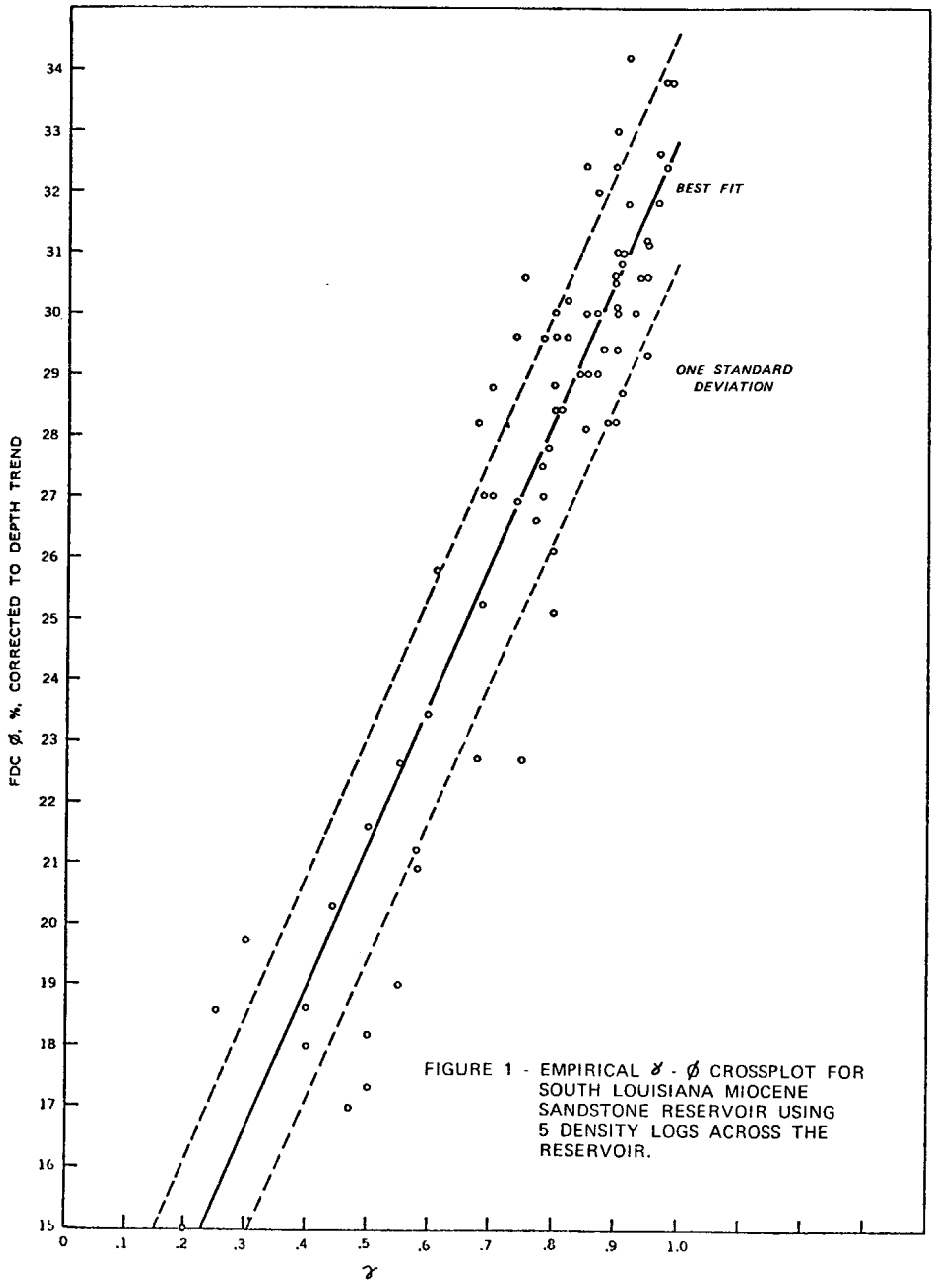

FIGURE 1 - EMPIRICAL γ - ϕ CROSSPLOT FOR SOUTH LOUISIANA MIOCENE SANDSTONE RESERVOIR USING 5 DENSITY LOGS ACROSS THE RESERVOIR.

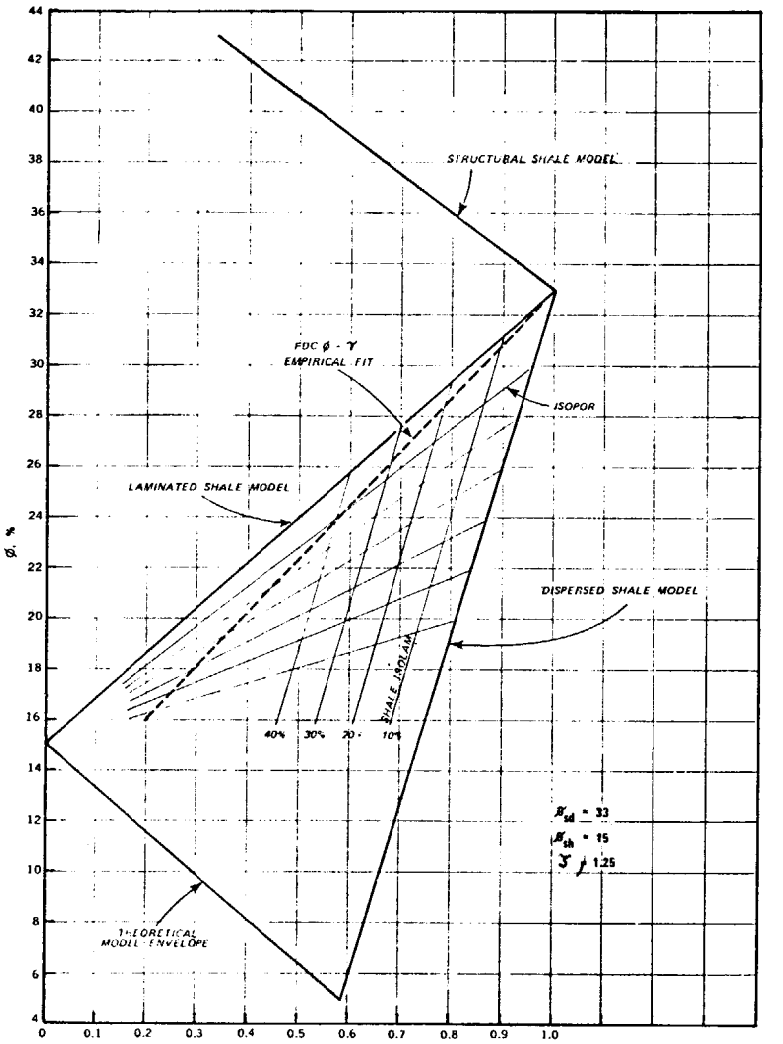

FIGURE 2 - THE THEORETICAL MODEL ENVELOPE FOR A SOUTH LOUISIANA SANDSTONE RESERVOIR WITH THE EMPIRICAL FIT AS THE DOTTED LINE, PREVIOUSLY SEEN IN FIGURE 1.

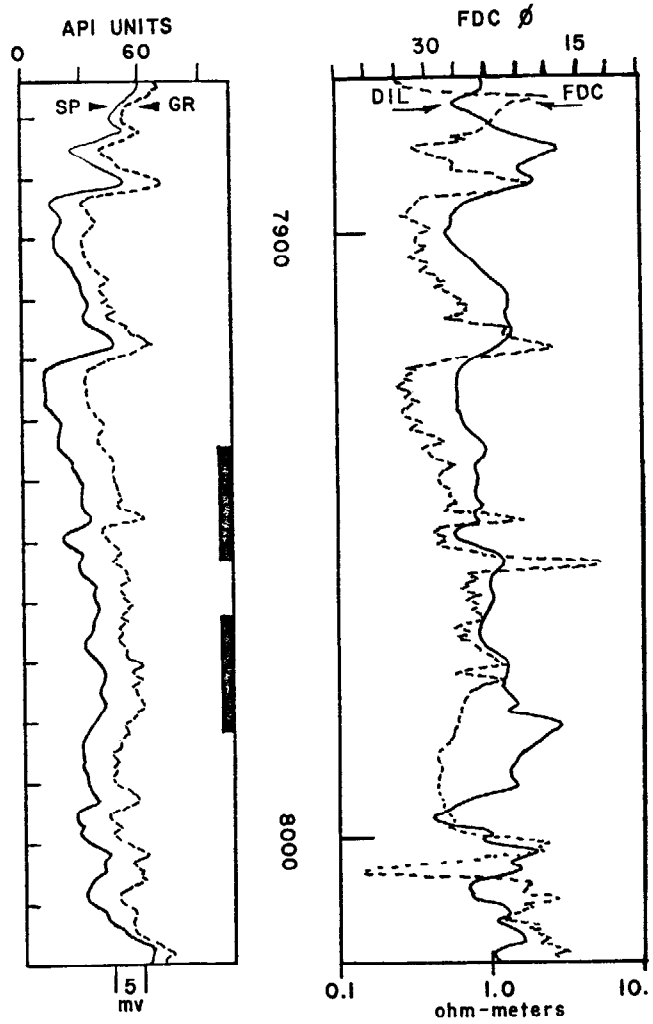

FIGURE 3 - PETROPHYSICAL SECTION FOR RESERVOIR IN SOUTH LOUISIANA, CORED INTERVAL SHOWN BY BAR IN TRACK I.

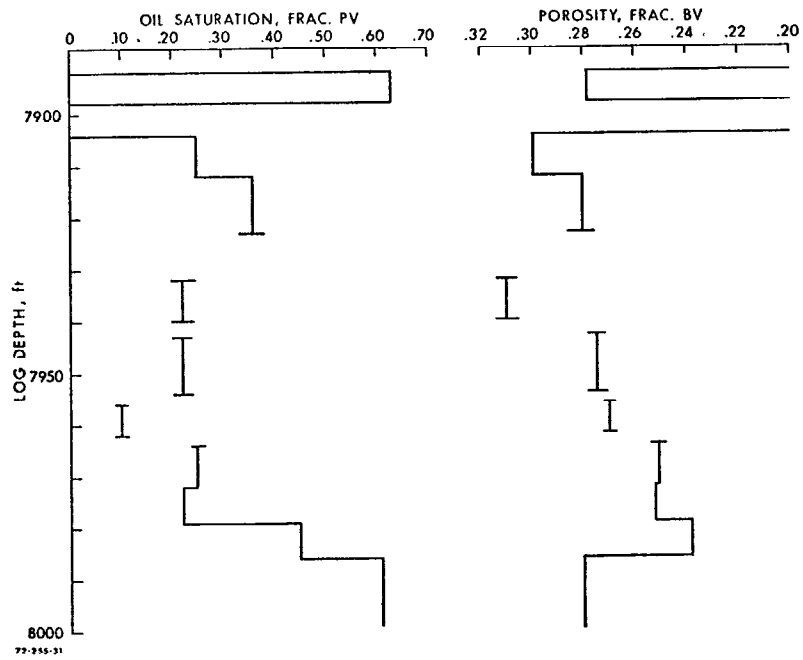

FIGURE 4 - OIL SATURATION-POROSITY PROFILE FROM DEEP INDUCTION AND DENSITY LOGS.

FIGURE 5 CORE PHOTOGRAPHS OF SOUTH LOUISIANA SANDSTONE RESERVOIR DEMONSTRATING THE PRESENCE OF SHALE LAMINATIONS.

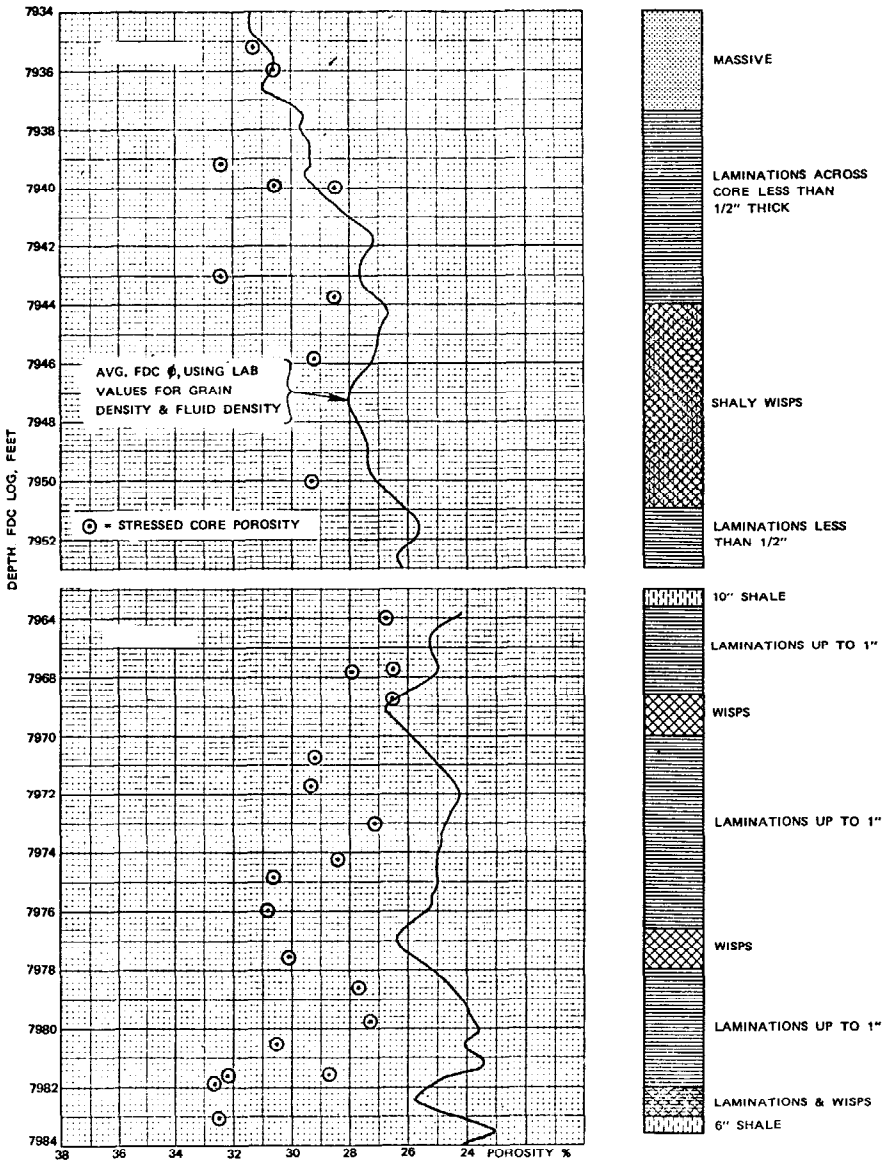

FIGURE 6 - FDC POROSITY & STRESSED CORE POROSITY DEMONSTRATING APPARENT DISCREPANCY BETWEEN ANALYSIS METHODS CAUSED BY LAMINATIONS.

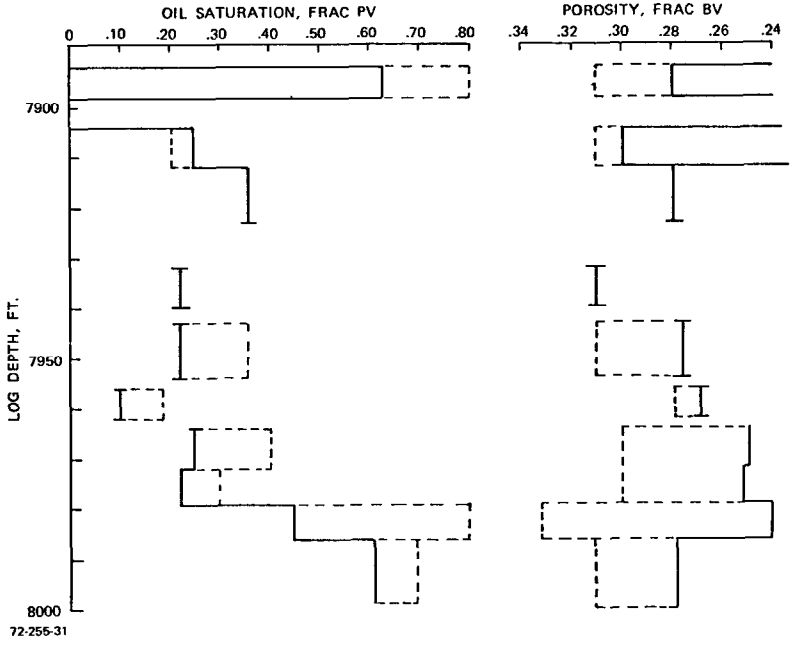

FIGURE 7 - OIL SATURATION-POROSITY PROFILE FROM DEEP INDUCTION AND DENSITY LOGS, SOLID LINE. CORRECTED FOR SHALY SAND EFFECTS ON INDUCTION & DENSITY SHOWN DOTTED LINE.